Available online at www.sciencedirect.com
SCIENCE DIRECT®
International Journal of Heat and Mass Transfer 49 (2006) 4043–4057
International Journal of HEAT and MASS TRANSFER
www.elsevier.com/locate/ijhmt

Numerical study of base effects on population inversion in DF chemical laser cavity

Jun Sung Park, Seung Wook Baek *

Division of Aerospace Engineering, Department of Mechanical Engineering, Korea Advanced Institute of Science and Technology, 373-1 Guseong-dong, Yuseong-gu, Daejeon 305-701, South Korea

Received 4 December 2003
Available online 9 June 2006

Abstract

Nowadays a chemical laser is globally studied and examined as a means of new high strategic weapon system or industrial equipment system. Different from the other laser systems, the chemical laser system has a great advantage in that a high power laser beam with megawatt range can be easily generated. In order to do that, the chemical laser system employs a supersonic mixing and chemical reaction in the cavity. In the DF chemical laser system, F atom as an oxidant and D_2 molecule as a fuel are injected and reacted so that the DF excited molecules are produced. These phenomena occur in a non-equilibrium state. The excited molecules are degenerated into the lower level energy states so as to generate the laser beam by means of the stimulated emission. Therefore, more excited molecules in higher energy level are desirable in order to generate a higher power laser beam by controlling a flow mixing and chemical reaction in the cavity. There are a lot of factors that may affect mixing and chemical reaction in producing excited molecules. Usually, the chemical laser system adopts a diffusion type of injection system with base. Thereby, a recirculation zone is formed behind the base which determines characteristics of mixing and chemical reaction. In this study, the effects of base height on the population inversion, that is one of the most important aspects in the chemical laser system, are numerically investigated. The results are discussed by considering three base heights of 0.4, 0.8 and 1.6 mm. Major results reveal that a transition of DF(1)–DF(0) as one of population inversions takes place in the whole range of cavity while its value decreases as the base height increases. On the contrary, the region over which the transitions of DF(2)–DF(1) and DF(3)–DF(2) occur, increases as the base height increases, while so does its value. Therefore, as the base height decreases, the maximum small signal gain (SSG) becomes higher in the v_{1-0} transition, whereas it becomes lower in the v_{2-1}, v_{3-2} and v_{4-3} transitions except in the nozzle inlet. Accordingly, the total extracted power is found to become higher with a decrease in base height.

Keywords: DF chemical laser; Population inversion; Lasing; Base; Supersonic flow

1. Introduction

Unlike other laser systems (solid state laser, semi-conductor laser, organic dye laser, etc.), the chemical laser produces the excited atoms or molecules by means of mixing and chemical reaction of fuel (H_2 or D_2) and oxidant (F) which is particularly supplied through the supersonic nozzle. The population inversion indispensable for generating laser beam only occurs in its cavity and this phenomenon strongly depends not only on the flow field properties, but also on the characteristics of mixing and chemical reaction.

For the case of DF chemical laser, some chemical species such as F, F_2, HF and He flow into the cavity through the supersonic nozzle with the Mach number of 4–5, while D_2 molecules are also injected into the cavity at the sonic speed. And then the species from the supersonic nozzle and D_2 molecules from the D_2 injector are mixed and reacted in the cavity. They are mixed in the recirculation

* Corresponding author. Tel.: +82 42 869 3714; fax: +82 42 869 3710.
E-mail addresses: jimmy@kaist.ac.kr (J.S. Park), swbaek@kaist.ac.kr (S.W. Baek).

0017-9310/$ - see front matter © 2006 Elsevier Ltd. All rights reserved.
doi:10.1016/j.ijheatmasstransfer.2006.03.037

Nomenclature

c	speed of light ($2.99792458 \times 10^{10}$ cm/s)
C_i	mass concentration of ith species (kg/m^3)
C_{pi}	specific heat at constant pressure of ith species (J/kg K)
E, F	inviscid flux vectors
E_v, F_v	viscous flux vectors
e_i	internal energy of ith species (J/kg)
e_t	total internal energy (J/kg)
h_i	enthalpy of ith species (J/kg)
I	intensity (W/m^2)
J	Jacobian, $\xi_x\eta_y - \eta_x\xi_y$
k	Boltzmann constant (5.670×10^{-8} W/m^2 K^4)
M	Mach number
n_i	ith species molar concentration (mol/m^3)
N_A	Avogadro number (mol^{-1})
P	mixture pressure (Pa)
Q	conservative state vector
R_u	universal gas constant (J/kmol K)
S	source vector
T	temperature (K)
t	time (s)
u, v	velocities (m/s)
x, y	Cartesian coordinates (m)
Y_i	ith species mass fraction
W_i	ith species molecular weight (kg/kmol)

Greek symbols

α	gain coefficient (cm^{-1})
ξ, η	generalized curvilinear coordinates
$\hbar$	Planck's constant ($6.6260755 \times 10^{-34}$ J s)
κ	thermal conductivity (J/m K s)
ρ	density (kg/m^3)
τ_{ij}	stress tensor
ν	transition frequency (s^{-1})
ω	transition frequency, ν/c (cm^{-1})

Superscript

–	non-dimensional quantities

Subscripts

i, j	space indices
J	rotational quantum number
ref	reference state
v	vibrational quantum number

zone formed behind the base. The term, 'base' which is usually used for the supersonic nozzle means a space between the nozzle lip and freestream. Similarly, the DF chemical laser system has a base located between the supersonic nozzle exit to provide the oxidant (F atom) and the D_2 injection holes. In general, the recirculation zone would significantly affect the mixing process so that the proper geometric base design is very important in determining the rate of mixing.

In 1970s, a lot of numerical and experimental studies regarding the chemical laser had been done. Spencer et al. [1] investigated the effects of H_2 and SF_6 mass flow variations and mirror open area on the laser power output as a preliminary study for the performance of HF chemical laser. A comparison of HF with DF continuous chemical laser was also presented by Spencer et al. [2]. In this study, the output power and the efficiency of conversion of chemical energy to laser energy were investigated for the chemical laser system in which population inversion is obtained by diffusing D_2 into a supersonic free jet containing F atoms.

The approximate theory characterizing diffusion flames in premixed systems was proposed for the chemical laser by Emanuel [3]. Especially, a behavior of premixed systems was examined for the cold reaction under constant pressure condition with one line lasing. The results revealed the parametric behavior of the system while discussing influential phenomena of j-shifting on the performance. King and Mirels [4] investigated the theoretical performance of an HF diffusion-type laser by studying the laminar diffusion of a finite stream of H_2 into a semi-infinite stream containing F and a diluent. Skifstad [5] presented a theory for an HF chemical laser by employing both the hot and cold pumping reactions under continuous wave conditions. The influence of the numerous parameters of the system on the specific power output, gain and saturation was also investigated. A simple model for a steady flow HF chemical laser was formulated by Broadwell [6], in which the excited state formation rate was limited by the H_2–F mixing rate. But its simple analytic prediction for lasers was markedly different from the experimental observations. Tripodi et al. [7] simulated the two dimensional flow of CW chemical laser and pointed out the need for a theoretical model that couples the effects of fluid mechanics on mixing with the non-equilibrium kinetics and the cascade of vibrational–rotational transitions. Ramshaw et al. [8] presented a new numerical method for calculating the steady-state output power and other operating characteristics of a continuous flow chemical laser.

In 1980s, Driscoll [9,10] performed experiments and numerical simulations to demonstrate the ability of a new supersonic ramp nozzle design to accelerate mixing in a DF chemical laser via the reactant surface stretching mechanism. Various types of nozzles were numerically investigated in the CW HF chemical laser by Hua et al. [11]. The flow properties, laser outcoupling power and small signal gain of a Fabry–Perot resonator were calculated considering four geometric parameters; throat width, area ratio, axis length and base. Also Shur [12] numerically studied a supersonic combustion in continuous HF chemi-

cal lasers with different nozzle designs, which is intended for separate delivery of fuel and oxidizer into the resonator cavity. The mechanism and degree of inverse effect of the processes occurring in the zone of mixing and combustion of supersonic jets were examined.

As mentioned before, the uniform and strong mixing characteristics play an important role in generating high power laser beam with high quality. Hence it is essential to understand influential factors that determine uniformity and strength of mixing in the chemical laser system. Therefore, in this study, the effects of base height, that is one of the most influential factors in determining the flow field properties, population inversion and lasing power in the DF chemical laser cavity as shown in Fig. 1, are investigated. Especially, the extent of rates of mixing and reaction as well as the size of population inversion zone is considered and discussed. To calculate the gas flow developments, the governing equations are non-dimensionalized and a fully conservative implicit and second order TVD schemes are used with the finite volume method (FVM). And an 11-species (including DF molecules at various excited states of energies), 32-step chemistry model is adopted for the DF reaction.

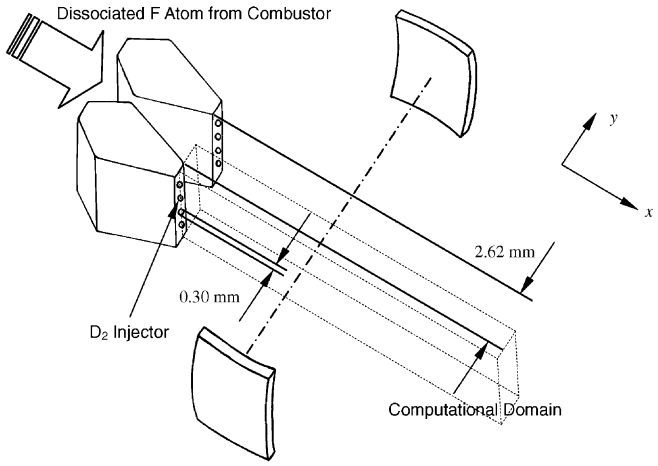

Fig. 1. Schematic of the supersonic diffusion DF chemical laser system.

2. Governing equations

The model is illustrated in Figs. 1 and 2, which show the DF chemical laser cavity block with the supersonic nozzle, D_2 injector and base. A uniform flow of F, F_2, HF and He enters the laser cavity resonator through the supersonic nozzle at $M = 5.0$, $P = 2.40$ Torr and $T = 169.37$ K in the upper domain, while the sonic D_2 flow is injected in parallel to it at $P = 192.0$ Torr and $T = 239.61$ K in the lower domain. Especially a base is placed between the supersonic nozzle and D_2 injector in order to control the rate of mixing. Behind it, a recirculation zone, in which flow is slowly circulating, is generated. The Reynolds number in this DF chemical laser system based on the supersonic nozzle conditions and its exit height (2.62 mm) is at most of the order of 10^3. And the Reynolds number based on the D_2 injector conditions and its height (0.3 mm) is also of the order of 10^2. Consequently, it is reasonable to assume that the flow in the DF chemical laser cavity is laminar.

2.1. Governing equations

The flow speed occurring in the DF chemical laser cavity block is approximately ranged from $M = 0$ to 5, so that the effects of compressible flow should be taken into account in the modeling. Hence, the governing equations for the above problem are the time-dependent compressible Navier–Stokes equations particularly in a strongly conservative form. The unsteady conservation equations are in the following form:

$$\frac{\partial Q}{\partial t} + \frac{\partial E}{\partial x} + \frac{\partial F}{\partial y} = \frac{\partial E_v}{\partial x} + \frac{\partial F_v}{\partial y} + S_{chem} + S_{rad}, \quad (1)$$

where Q is the conservative flow variable vector, and E and F are the inviscid flux vectors in the x, y directions, respectively. E_v and F_v are the viscous flux vectors. Finally, S_{chem} and S_{rad} are source vectors that indicate the rates of formation of chemical species due to the chemical reaction and the stimulated emission, respectively. Each vector is defined as below:

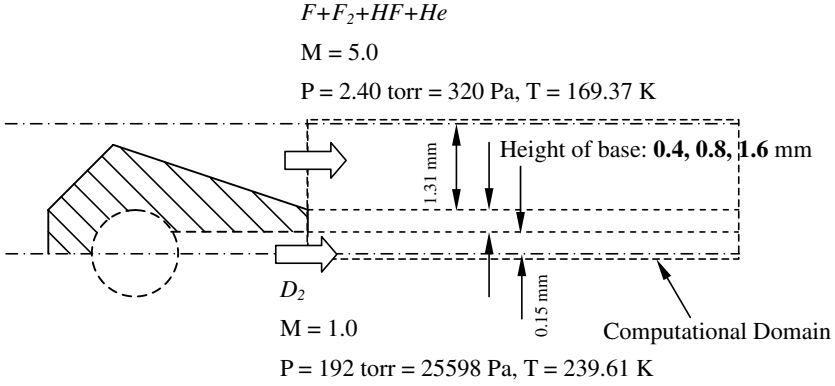

Fig. 2. Schematic of the supersonic nozzle, D_2 injector and base in the DF chemical laser cavity.

$$Q=\begin{bmatrix}\rho\\ \rho u\\ \rho v\\ \rho e_{\mathrm{t}}\\ \rho Y_i\end{bmatrix},\quad E=\begin{bmatrix}\rho u\\ \rho u^2+P\\ \rho uv\\ u(\rho e_{\mathrm{t}}+P)\\ \rho uY_i\end{bmatrix},\quad F=\begin{bmatrix}\rho v\\ \rho uv\\ \rho v^2+P\\ v(\rho e_{\mathrm{t}}+P)\\ \rho vY_i\end{bmatrix},$$

$$E_{\mathrm{v}}=\begin{bmatrix}0\\ \tau_{xx}\\ \tau_{xy}\\ u\tau_{xx}+v\tau_{xy}-q_x+q_{\mathrm{sx}}\\ d_x\end{bmatrix},$$

$$F_{\mathrm{v}}=\begin{bmatrix}0\\ \tau_{xy}\\ \tau_{yy}\\ u\tau_{xy}+v\tau_{yy}-q_x+q_{\mathrm{sy}}\\ d_y\end{bmatrix},\quad S_{\mathrm{chem}}=\begin{bmatrix}0\\ 0\\ 0\\ 0\\ \omega_i\end{bmatrix},$$

$$S_{\mathrm{rad}}=\begin{bmatrix}0\\ 0\\ 0\\ -\sum_v\sum_J \alpha_{v,J}I_{v,J}\\ \omega_{\mathrm{rad},i}\end{bmatrix}.$$

By considering a mixture of multi-species, the term of e_{t} in Eq. (1) becomes

$$e_{\mathrm{t}}=\sum_{i=1}^{\mathrm{NS}}Y_ih_i-\frac{P}{\rho}+\frac{1}{2}\left(u^2+v^2\right), \tag{2}$$

$$h_i=h_{\mathrm{f}i}^0+\int_{T_{\mathrm{ref}}}^{T}C_{p_i}\,\mathrm{d}T, \tag{3}$$

$$P=\rho R_{\mathrm{u}}T\sum_{i=1}^{\mathrm{NS}}\frac{Y_i}{W_i}, \tag{4}$$

where NS in Eqs. (2) and (4) represents the number of chemical species involved in the chemical reactions.

q_{x_i} and q_{sx_i} in the energy equation, and d_{x_i} in the species equations can be denoted by

Table 1
DF chemical laser inlet conditions

	Upper nozzle		D_2 injector	
Mach number		5.0		1.0
Temperature (K)		169.37		239.61
Pressure (Torr)		2.40		192.00
Species	F	0.3071	D_2	1.0
Mass fraction	F_2	0.0340		
	HF	0.3191		
	He	0.3398		

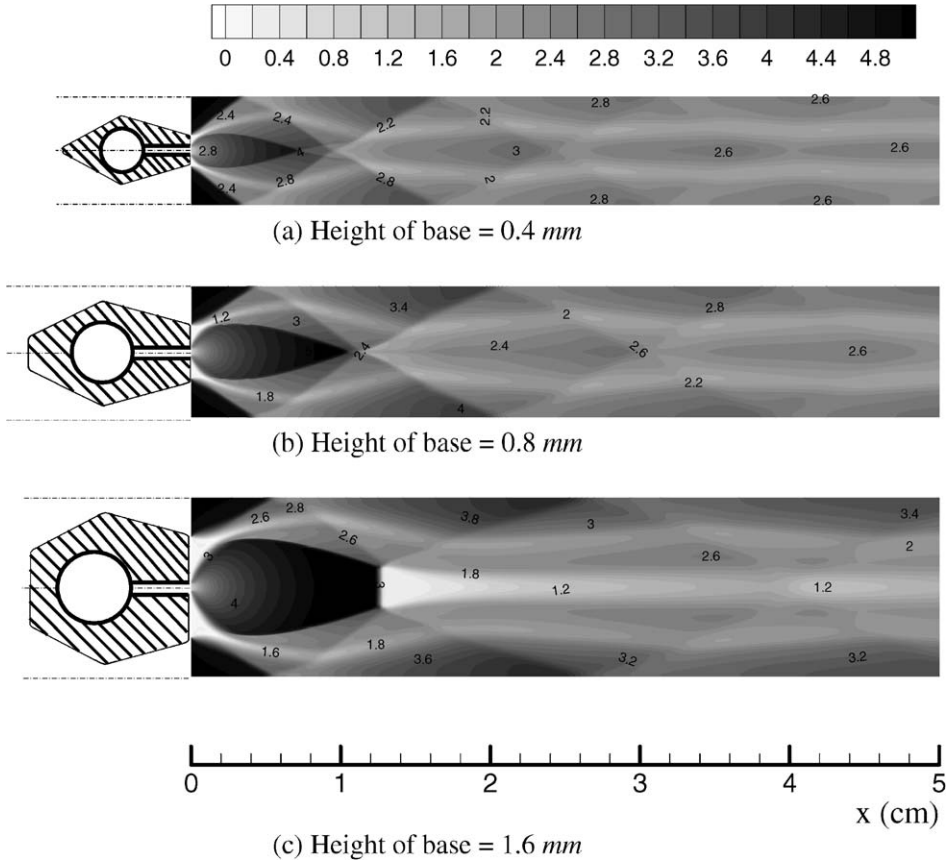

Fig. 3. Effects of the heights of base on the Mach contours.

$$q_{x_i} = -k\frac{\partial T}{\partial x_i}, \tag{5}$$

$$q_{sx_i} = \sum_{j=1}^{NS} D_{jm} h_j C_j \frac{\partial Y_j}{\partial x_i}, \tag{6}$$

$$d_{x_i} = \rho D_{jm} \frac{\partial Y_j}{\partial x_i}, \tag{7}$$

where D_{jm} is the diffusion coefficient of jth chemical species in gas mixture. q_{x_i} and q_{sx_i} represent the conduction heat flux and the heat generation due to chemical reaction, respectively. More details on the source vectors S_{chem} and S_{rad} will be mentioned in the following sections of the chemical reaction model and the radiative transfer equation.

To close the system of Eq. (1), the equation of state needs to be introduced. The macroscopic thermodynamic properties of the gas are related through the general equation of state,

$$P = P(\rho, e, C_1, C_2, \ldots, C_{NS-1}) = R_u T \sum_{i=1}^{NS} \frac{C_i}{W_i} = R_u T \left\{ \frac{\rho}{W_{NS}} + \sum_{i=1}^{NS-1} C_i \left(\frac{1}{W_i} - \frac{1}{W_{NS}} \right) \right\}, \tag{8}$$

$$\rho = \sum_{i=1}^{NS} \rho Y_i = \sum_{i=1}^{NS} C_i. \tag{9}$$

2.2. Chemical reaction model

Besides thermo-chemical and fluidic conditions imposed, the chemical reaction model would play an extremely important role in analyzing the DF chemical lasing processes. Because a high speed gas is expanding through a supersonic nozzle into the cavity in a very short time, its phenomena may not be simply described by the single step chemical reaction. Instead the multi-step chemical reaction model has to be applied as follows:

$$\sum_{j=1}^{NS} v'_{ij} n_j \underset{k_{b_i}}{\overset{k_{f_i}}{\rightleftharpoons}} \sum_{j=1}^{NS} v''_{ij} n_j, \quad i = 1, 2, \ldots, N_R, \tag{10}$$

where v'_{ij} and v''_{ij} represent the stoichiometric coefficients of the jth reactants and products for ith chemical reaction step. n_j is the molar concentration of the jth species and N_R is the total number of the chemical reaction step. k_{fi} and k_{bi} are the forward and backward reaction rate constants, which are experimentally determined and expressed by the Arrhenius type as follows:

$$k_i = A_i T^{m_i} e^{-E_i/R_u T}, \tag{11}$$

where E_i is the activation energy, and A_i and m_i are all determined using experimental data.

For the chemical reaction (10), the rate of change of mass concentration for the jth species becomes

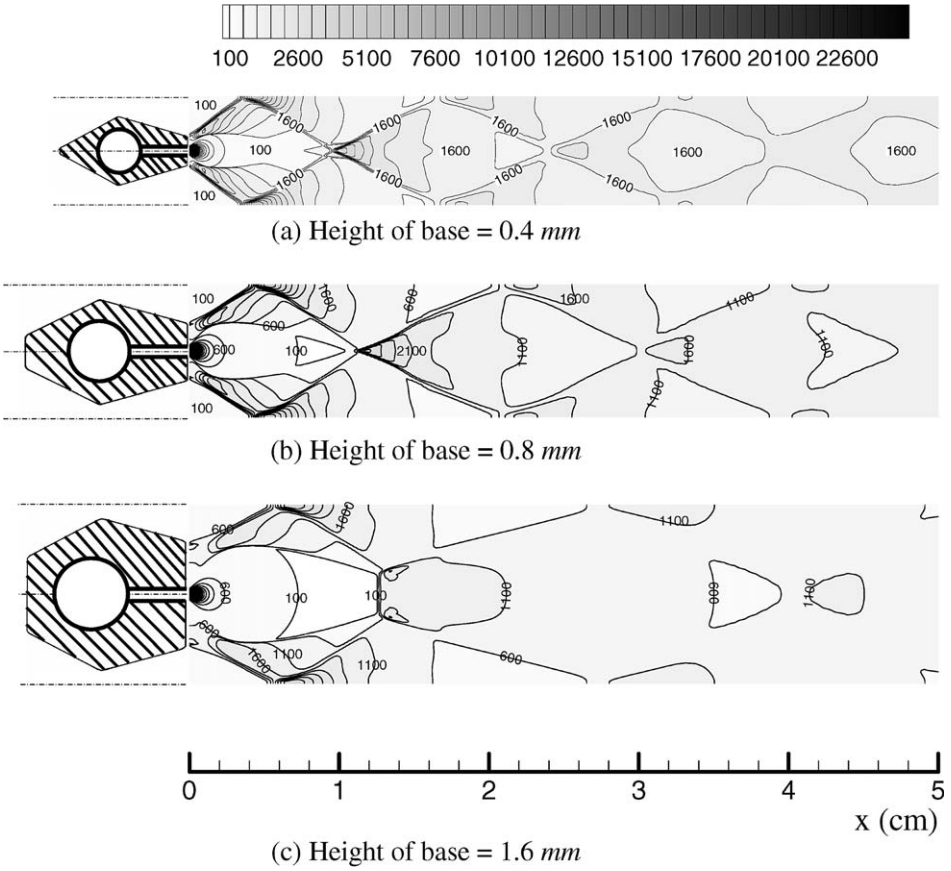

Fig. 4. Effects of the heights of base on the pressure contours.

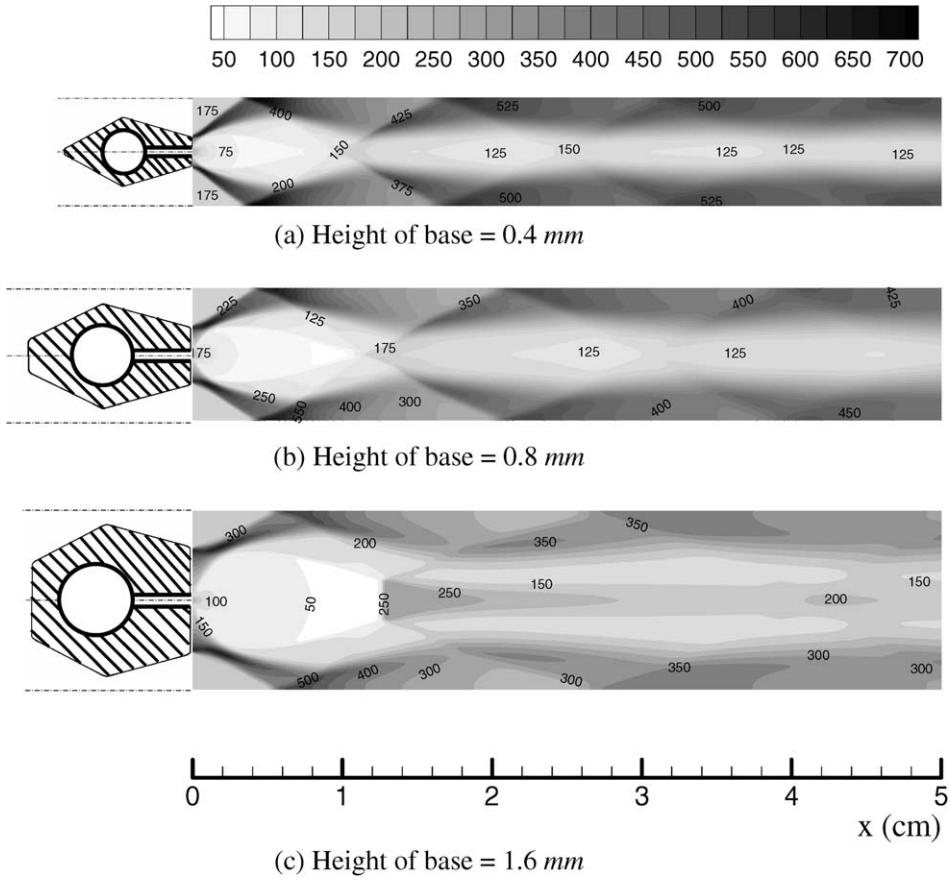

Fig. 5. Effects of the heights of base on the temperature contours.

$$\omega_j = W_j \sum_{i=1}^{N_R} \left[\left(v''_{ij} - v'_{ij} \right) \left(k_{fi} \prod_{l=1}^{NS} n_l^{v'_{il}} - k_{bi} \prod_{l=1}^{NS} n_l^{v''_{il}} \right) \right]. \quad (12)$$

In the present study, the 32-step chemistry model for 11-species (including DF molecules in various excited states), is adopted for the DF reaction occurring in cavity. Especially, a variety of vibrational energy states of the DF excited molecules are considered as the individual molecules like DF(0), DF(1),..., DF(4). Also, under the assumption of an equilibrium Boltzmann distribution for the rotational populations at the translational temperature T, the rotational energy states for each vibrational state are indicated by

$$\rho_{v,J} = \rho_v \frac{2J+1}{Q(v)} \exp\left(-\frac{\hbar c}{k} \frac{E_{v,J}}{T} \right), \quad (13)$$

where $Q(v)$ is the rotational–partition function for vibrational level v, c is the speed of light, k is the Boltzmann constant, and $E_{v,J}$ is the rotational energy of state v, J. Therefore, only translational temperature is used to obtain the distribution of the DF excited molecule at each quantized vibrational and rotational state.

2.3. Radiative transport equation

A monochromatic, unidirectional light emitted by a laser is electromagnetic radiation. Therefore, in order to analyze the laser beam characteristics and its power, the radiative transport equation is needed to deal with the electromagnetic radiation. The fundamental equation for radiative transfer in the laser cavity can be written by

$$\pm \frac{\partial I^{\pm}_{v,J}}{\partial y} = \alpha_{v,J} I^{\pm}_{v,J}, \quad (14)$$

where $I^{\pm}_{v,J}$ is the intensity of radiation in the spectral line from $(v+1, J-1)$ to (v, J) propagating in the y-direction. And $\alpha_{v,J}$ is the optical gain coefficient that is evaluated by Gross and Bott [13]. Assuming that the plane-parallel mirrors are located at both end sides of y-axis, the appropriate boundary conditions are

$$I^{+}_{v,J} = r_0 I^{-}_{v,J} \quad \text{at } y = 0, \qquad I^{-}_{v,J} = r_{L_{axis}} I^{+}_{v,J} \quad \text{at } y = L_{axis}, \quad (15)$$

where r_0 and $r_{L_{axis}}$ are the mirror reflectivities of which values used in this system are, respectively, 0.87 and 1.0.

$\omega_{rad,i}$ in the source vector S_{rad} of species equation (1) illustrates the rate of formation of ith chemical species due to the stimulate emission. However, this term is not zero only when the chemical species are DF molecules in the DF chemical laser. Its rate of formation of the excited DF molecule is expressed as follows:

$$\omega_{rad,i} = \frac{W_{DF}}{\hbar N_A} \sum_J \left(\frac{\alpha_{v,J} I_{v,J}}{\nu_{v,J}} - \frac{\alpha^{v,J} I^{v,J}}{\nu^{v,J}} \right). \quad (16)$$

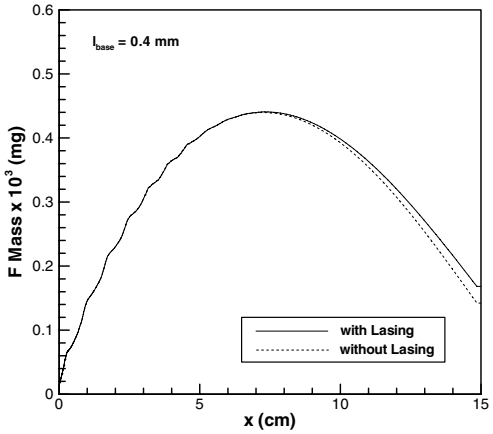

(a) Height of base = 0.4 *mm*

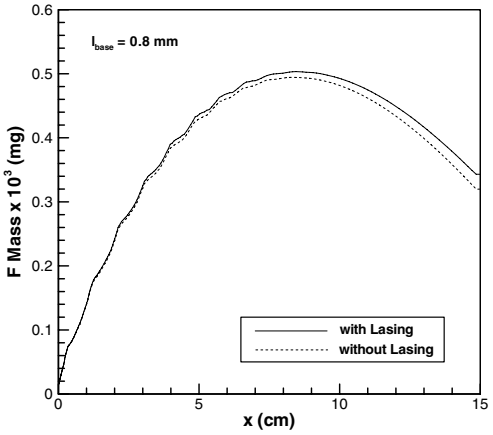

(b) Height of base = 0.8 *mm*

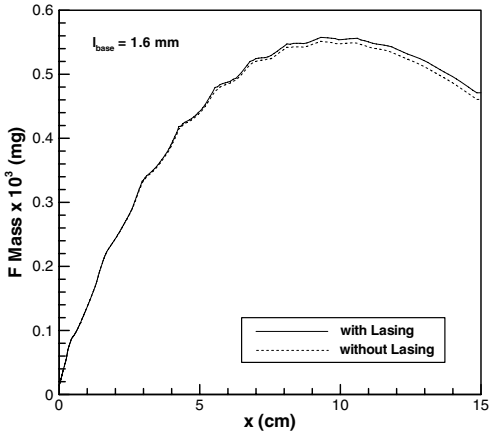

(c) Height of base = 1.6 *mm*

Fig. 6. Comparison of F atom mass distributions with respect to longitudinal distance x from the nozzle exit plane.

The subscript or superscript v, J represents a P-branch transition from $(v+1, J-1)$ to (v, J) or the one from (v, J) to $(v-1, J+1)$, respectively.

3. Numerical method

In order to predict a variation of thermo-fluid dynamic as well as species distributions, Eq. (1) governing physical phenomena in DF chemical laser cavity is to be discretized. There exist a lot of numerical methods for solving this type of systems. In the present analysis, the finite volume method (FVM) is employed since it is known to easily satisfy the conservation rules and to be computationally stable at the surface of discontinuities.

First of all, a physical domain is transformed to a computational domain in order to promote the numerical efficiency and conveniently apply the physical boundary conditions using the following coordinate transformation

$$\xi = \xi(x, y), \tag{17}$$

$$\eta = \eta(x, y). \tag{18}$$

After the coordinate transformation, Eq. (1) becomes

$$\frac{\partial \overline{Q}}{\partial t} + \frac{\partial \overline{E}}{\partial \xi} + \frac{\partial \overline{F}}{\partial \eta} = \frac{\partial \overline{E}_v}{\partial \xi} + \frac{\partial \overline{F}_v}{\partial \eta} + \overline{S}, \tag{19}$$

where

$$\overline{Q} = \frac{1}{J} Q, \quad \overline{E} = \frac{1}{J}\left(\xi_x E + \xi_y F\right), \quad \overline{F} = \frac{1}{J}\left(\eta_x E + \eta_y F\right),$$

$$\overline{E}_v = \frac{1}{J}\left(\xi_x E_v + \xi_y F_v\right), \quad \overline{F}_v = \frac{1}{J}\left(\eta_x E_v + \eta_y F_v\right), \quad \overline{S} = \frac{1}{J} S,$$

while the Jacobian, J represents the volume of each cell in the Cartesian coordinate system.

In order to solve the Navier–Stokes equations in the generalized coordinate, the Roe's average [14] and the second order TVD (total variation diminishing) scheme [15,16] are used together with the finite volume method (FVM), thereby improving the resolution of discontinuities in a reacting compressible flow. For TVD scheme, the limiter employed is a less compressive van Leer limiter for non-linear fields, while a more compressive superbee limiter is used for the linear fields. And the entropy correction [15,16] is used for $\delta = 0.01$ in order to prevent the unphysical solutions from occurring through correcting the eigenvalues in the flux Jacobian matrix.

3.1. Time stepping method

In order to solve the constitutive equations with the conservative vector variables, the LU decomposition proposed by Jameson and Turkel [17] is adopted here, since it has the advantage in reducing the computational efforts in calculating the inverse matrices. In this study, the numerical results are the steady state solutions simulating the DF chemical laser cavity so that the local time stepping method is chosen in order to rapidly achieve the numerical solution.

3.2. Boundary conditions

Fig. 2 shows a schematic configuration of the DF chemical laser cavity that comprises the supersonic nozzle and D_2 injector with base. The half lengths of the supersonic nozzle and D_2 injector are 1.31 mm and 0.15 mm, respectively, whereas the base height is varied to investigate its

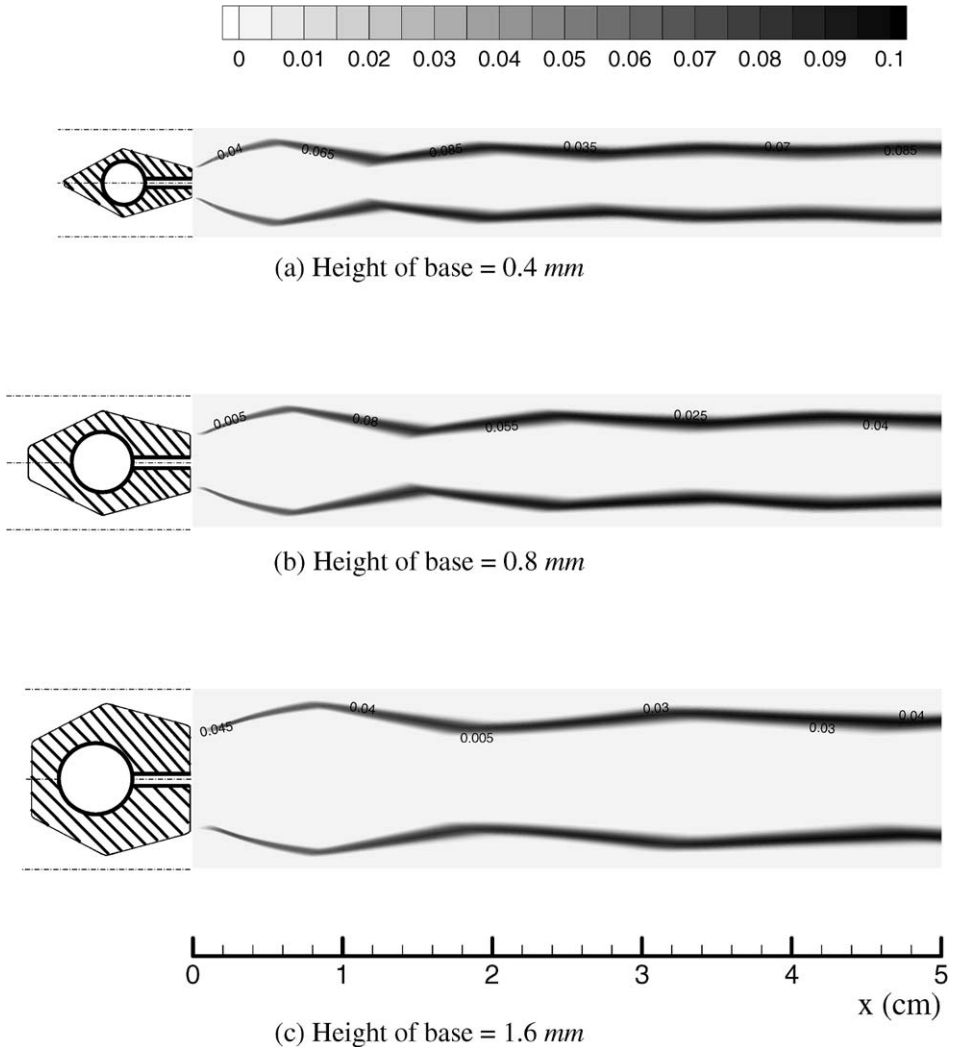

Fig. 7. Effects of the heights of base on the DF(3) mass fraction contours.

effects on the population inversion. The different grid system is used according to the base size such that 301×101 for 0.4 mm base, 301×125 for 0.8 mm base and 301×151 for 1.6 mm base. These grid systems are chosen after many preliminary calculations with different grid sizes.

For an analysis of the laser cavity, the boundary conditions have to be applied to upper and lower walls, inlet and outlet as shown in Fig. 2. At upper and lower walls, the symmetric condition is imposed since the physical domain is a part of the nozzle array. At the outlet, the outflow condition of the 0th order extrapolation is used, because the flow moves at the supersonic speed. At the inlet the conditions at the supersonic nozzle and the D_2 injector as tabulated in Table 1 are employed and these conditions are from the experiments of a real DF chemical laser system in the Agency for Defense Development. At the nozzle base the adiabatic condition is applied.

In order to calculate the intensity distributions, the boundary conditions expressed in Eq. (15) are applied. The cavity block is supposed to consist of 10 nozzle blocks in the y-direction. The resonator is equipped with two flat mirrors of which separate distances are 37.2, 45.2 and 61.2 mm for 0.4, 0.8 and 1.6 mm in base height, respectively. The width of a mirror is 5 cm while one end of the mirror is located at the nozzle exit ($x = 0$ cm).

4. Results and discussion

Especially a chemical laser system has such an advantage that high power laser beam can be generated in megawatt range, compared with other laser systems. Generally a laser beam is generated by means of the stimulated emission, in which an atom in an upper energy level interacts with incoming light so that it is stimulated to drop to a lower energy level and emit the energy difference as light. This process is much less familiar than either fluorescence or absorption, but it is the process that is required for laser operation. In order to make the stimulated emission stronger, the number of atoms or molecules in an upper energy level has to increase more than that in a lower energy level. It is called the population inversion, which is a non-equilib-

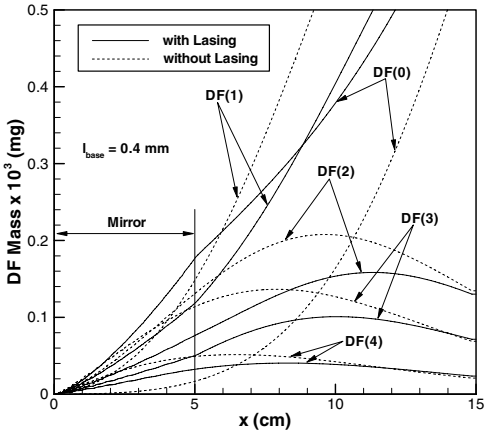

(a) Height of base = 0.4 *mm*

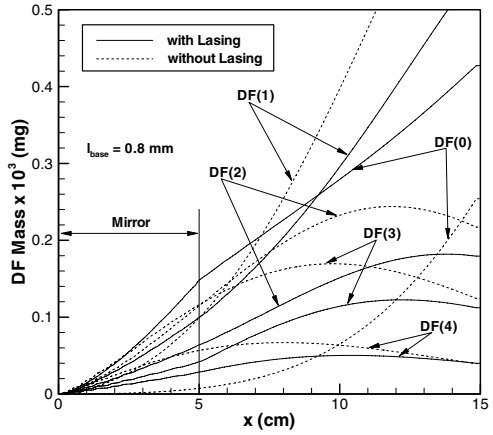

(b) Height of base = 0.8 *mm*

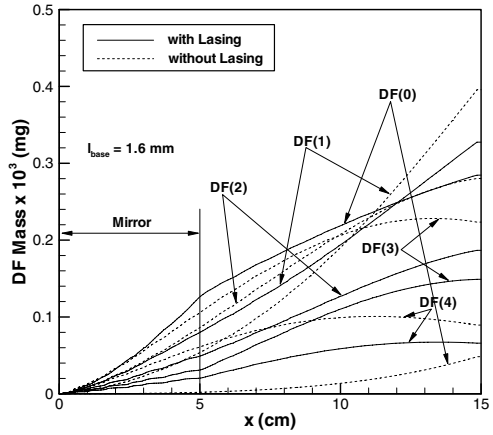

(c) Height of base = 1.6 *mm*

Fig. 8. Effects of the base heights on the mass distributions of the excited DF molecules with respect to longitudinal distance x from the nozzle exit plane.

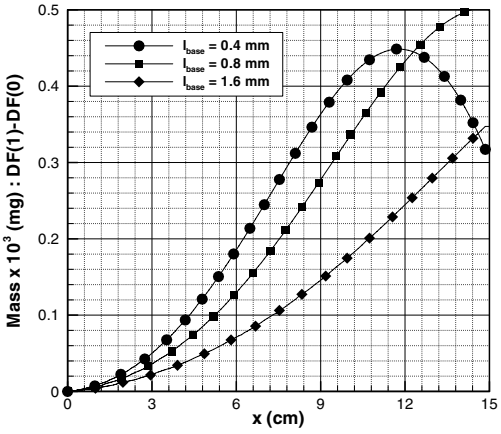

(a) DF(1)-DF(0)

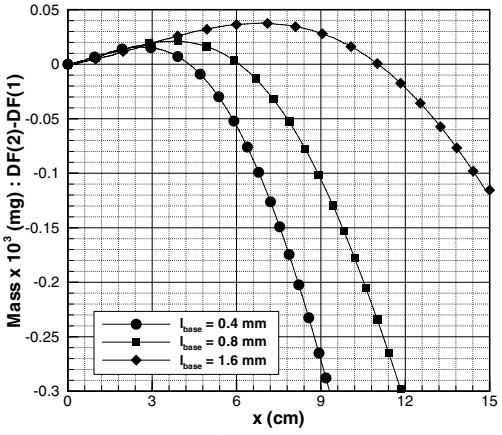

(b) DF(2)-DF(1)

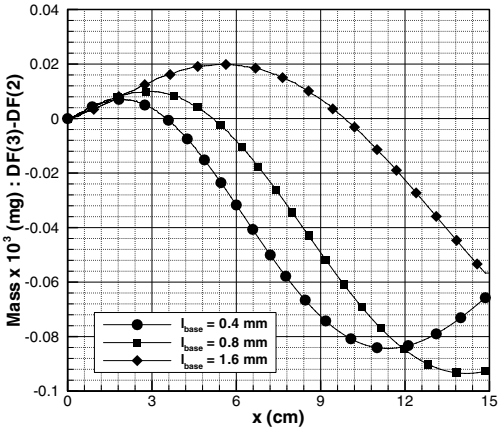

(c) DF(3)-DF(2)

Fig. 9. Effects of the base heights on the mass distributions of DF(i)–DF($i-1$) ($i = 1$–3) with respect to longitudinal distance x from the nozzle exit plane for the cases without lasing.

rium phenomenon such that the atoms or molecules in an upper energy level finally drop to a lower energy level, eventually reaching an equilibrium state. In this process, photons (a kind of energy wave) are generated. As the amount of atoms or molecules in an upper energy level increases, the intensity of light (energy of photon) becomes stronger.

The chemical laser cavity comprises a supersonic nozzle for providing oxidant, an injector for supplying fuel and a base for mixing and generating chemical reaction in order to bring about population inversion in a limited domain as shown in Fig. 2. The extent of mixing and chemical reaction in the laser cavity has a direct impact on the population inversion, so that developing a geometric design of

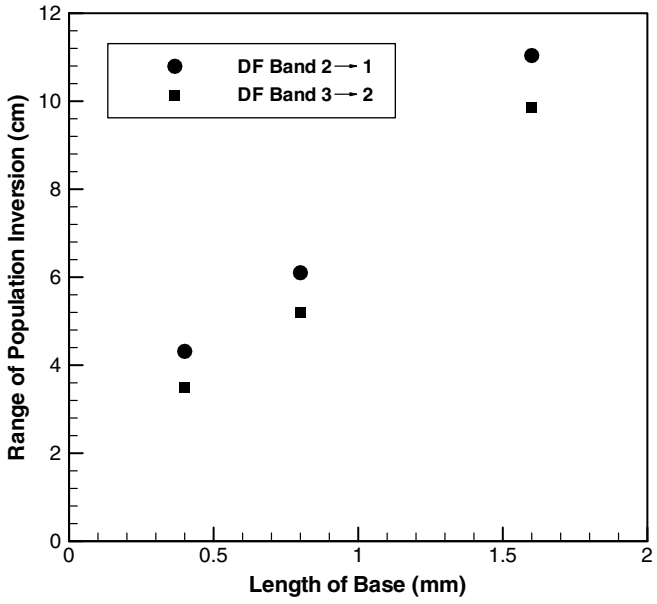

Fig. 10. Range of population inversion versus base heights.

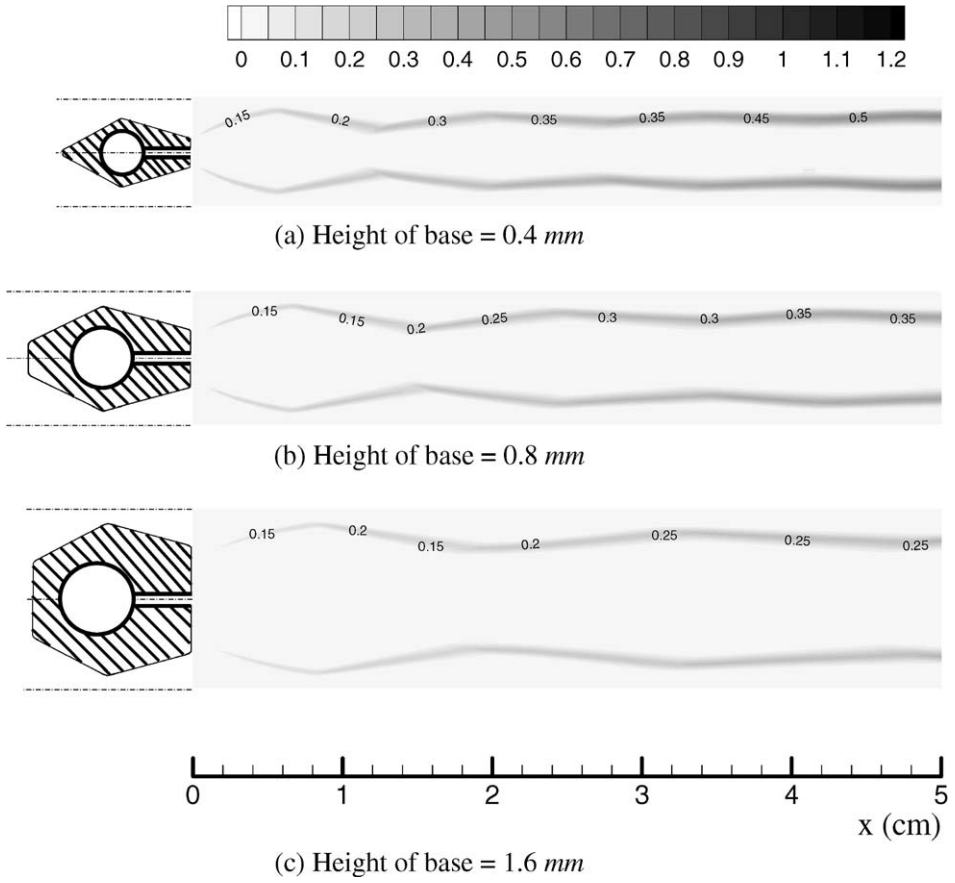

Fig. 11. Effects of the heights of base on the maximum small signal gain (DF(1)–DF(0)) contours.

high-performance cavity is an important factor in determining the strength of laser beam. In the present study, the distributions of the excited DF molecules, D_2 molecules (fuel) and F atoms (oxidant) are to be numerically predicted with the developed code [18], since they are good indicators representing corresponding status of population

inversion. Then, variations of the flow field characteristics as well as the small signal and saturated gains are discussed in order to analyze the effects of geometric design of base on the population inversion in the DF chemical laser cavity, while considering a laser power generation.

Figs. 3–5 show variations of Mach number, pressure and temperature when the base height is changed. Starting from the D_2 injection, the flow expansion in spanwise as well as in streamwise direction is observed to become wider as the base height increases. As shown in Fig. 3, the D_2 flow is accelerating, while F flow is decelerating. Especially there exists a Mach disc only for the case of 1.6 mm in base height, across which flow properties such as pressure, temperature and density abruptly increase, while the Mach number suddenly decreases. After the Mach disc, the shock reflection angle is more declined only for the case of 1.6 mm in base height. Consequently the characteristics of mixing, chemical reaction and population inversion would be different for this case due to the specific features of Mach patterns, which is to be discussed in more detail in the below.

On the other hand, the recirculation zone, in which the Mach number is very low, is generated behind the base and its area becomes wider as the base height increases. A large area of recirculation zone makes the rates of mixing and reaction of F atom as an oxidant and D_2 molecule as a fuel fall down in the vicinity of the inlet domain.

Effects of the base height on the pressure distributions are explained in Fig. 4, which reveals that the pressure after a couple of shock wave reflections becomes higher as the base height is smaller. That is, the smaller the base height, the stronger the shock wave interaction becomes. Also the Mach disc as well as more declined angle of shock wave reflection observed above for the case of 1.6 mm base height is clearly shown in Fig. 4(c). Fig. 5 illustrates variations of temperature distributions with the base height. As the base height becomes smaller, the temperature in the entire domain is seen to increase, which results from the flow interaction with strong shock wave reflection. Based on these, the chemical reaction and the population inversion would be more activated for smaller base height.

Fig. 6 shows the mass distributions of F atom (oxidant) along the longitudinal distance x from the nozzle exit plane. The mass means the sum of the F species mass distributed in y–z plane at the location, x. The distributions of F atom reveal that as the height of base becomes smaller,

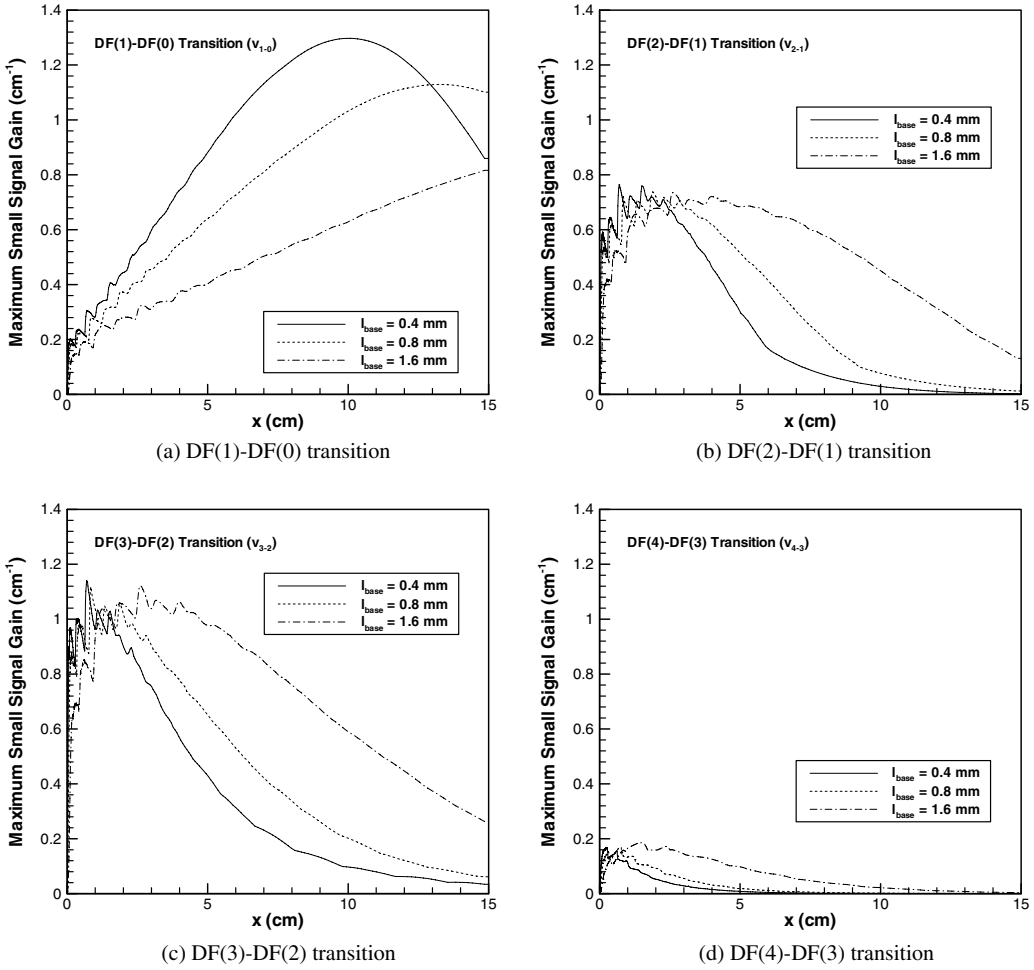

(a) DF(1)-DF(0) transition

(b) DF(2)-DF(1) transition

(c) DF(3)-DF(2) transition

(d) DF(4)-DF(3) transition

Fig. 12. Maximum small signal gain distributions with respect to longitudinal distance x from the nozzle exit plane.

the consumption of an oxidant (F atom) increases. The reason is that a stronger shock wave interaction for a smaller base height makes the local temperature higher so that a higher-energy species is more activated. However, the depletion of F atom decreases when the laser beam is being generated. This is because the negative stimulated emission term in the energy equation (1) makes the local temperature lower due to lasing so that the chemical reaction becomes a little weakened.

The distribution of the DF(3) mass fraction is considered to be a representative excited molecule in the DF chemical laser system so that it is plotted in Fig. 7. The species of DF(3) is distributed in thin zone along the downstream and is almost overlapped over the shock reflection trajectory. In this reaction zone, a more excited DF species is found for smaller base height, since the activated reaction zone shifts farther upstream.

All the excited DF molecules (from DF(0) to DF(4)) are illustrated in Fig. 8 along the axial distance x from the nozzle exit plane. When the lasing occurs, the excited DF molecules degenerate into the lower energy level so that a normal distribution of the excited DF molecules is found such that (DF(0) > DF(1) > DF(2) > DF(3) > DF(4)). However, out of the resonator, the population inversion between DF(0) and DF(1) comes about again and this phenomenon happens closer to the resonator for the smaller base height. For the case without lasing, the population inversion can be observed in much wider region and its range becomes wider as the height of base increases, which can be also confirmed in Figs. 9 and 10. Fig. 9 reveals that the population inversion in the transition of DF(1)–DF(0) takes place in the whole range and its strength becomes weaker as the base height increases. However, for the transitions of DF(2)–DF(1) and DF(3)–DF(2), the population inversion takes place over the wider region and the differences (DF(i)–DF($i-1$)) also becomes bigger as the base height increases. Especially, the ranges for population inversion in the transitions of DF(2)–DF(1) and DF(3)–DF(2) are plotted against the base height in Fig. 10, based on the data in Fig. 9. As the base height increases, the domain for population inversion increases almost linearly for the transitions; DF(2)–DF(1) and DF(3)–DF(2). And the domain for the population inversion from DF(2) to DF(1) is always longer than that from DF(3) to DF(2).

For the v_{1-0} transition, Fig. 11 illustrates the effects of the base height on the maximum small signal gain (SSG),

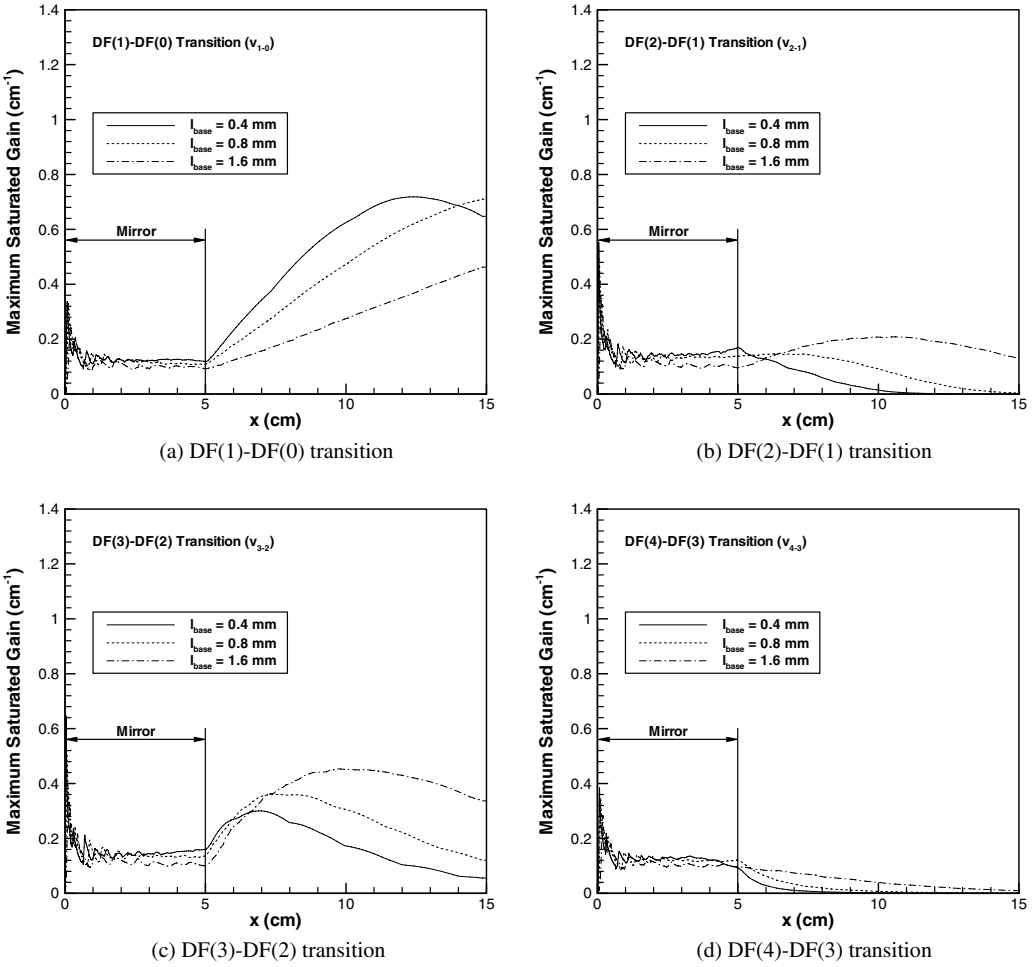

(a) DF(1)-DF(0) transition

(b) DF(2)-DF(1) transition

(c) DF(3)-DF(2) transition

(d) DF(4)-DF(3) transition

Fig. 13. Maximum saturated gain distributions with respect to longitudinal distance x from the nozzle exit plane.

which is commonly a principal factor in determining the laser beam power. The reason is that for each vibrational transition from $v+1$ to v, at most one line can lase in steady state and this will be the line of highest gain [8]. In the v_{1-0} transition, the maximum SSG becomes higher as the base height decreases. As a matter of fact, it is also observed that the distance between the reaction zone and the D_2 injector axial line becomes longer due to a larger recirculation zone, as the base height increases.

Fig. 12 quantitatively shows an axial distribution of maximum SSG from the nozzle exit plane. The maximum SSG distributions are directly related to the data from Fig. 9, since the SSG is calculated with the DF species concentrations, ρ_v using

$$\alpha_{v,J} = \left(\frac{\hbar N_A}{4\pi W_{DF}}\right)\omega\phi B(v,J)(2J+1) \times \left\{\frac{\rho_{v+1}}{Q(v+1)}\exp\left(-\frac{\hbar c}{\kappa}\frac{E_{v+1,J-1}}{T}\right) - \frac{\rho_v}{Q(v)}\exp\left(-\frac{\hbar c}{\kappa}\frac{E_{v,J}}{T}\right)\right\}, \quad (20)$$

where ϕ is a Doppler broadening line profile function, Q is a rotational partition function for each vibrational level and $E_{v,J}$ is a rotational–vibrational energy at the (v,J) state [13]. And $B(v,J)$ is a matrix related to the Einstein coefficient, $|M_l^u|^2$ and can be expressed by

$$B(v,J) = \frac{16\pi^4}{3\hbar^2 c}\left(\frac{2J}{2J+1}\right)|M_l^u|^2. \quad (21)$$

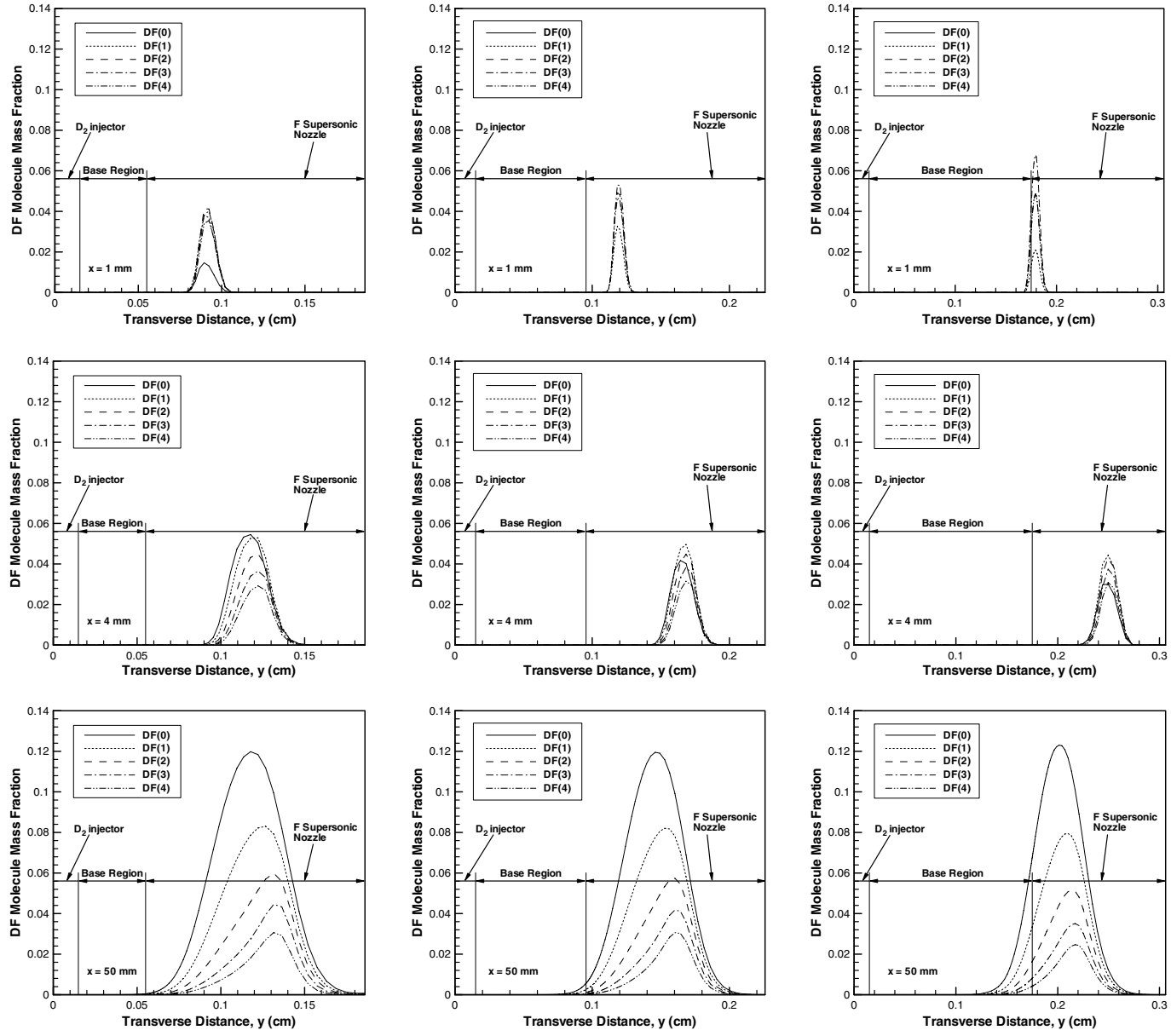

(a) $l_{Base} = 0.4$ *mm* (b) $l_{Base} = 0.8$ *mm* (c) $l_{Base} = 1.6$ *mm*

Fig. 14. Transverse distributions of various DF species at $x = 1$, 4 and 50 mm from the nozzle exit plane.

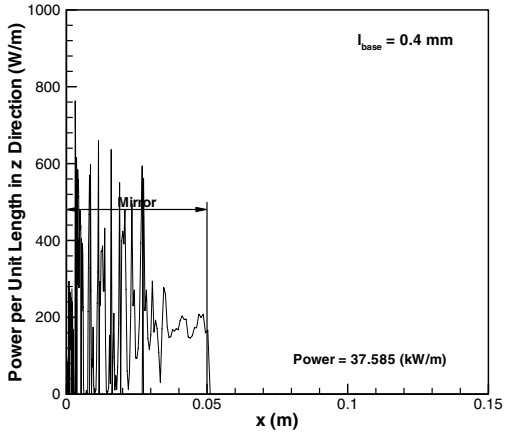

(a) Height of base = 0.4 *mm*

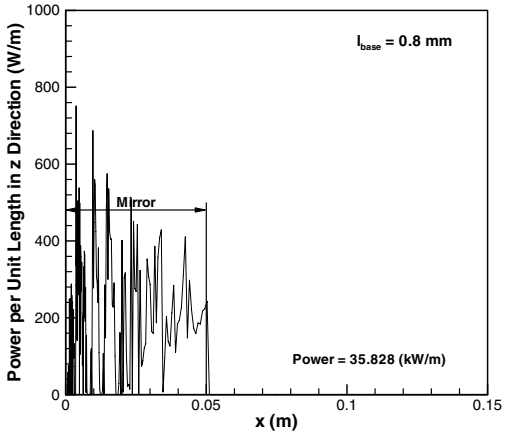

(b) Height of base = 0.8 *mm*

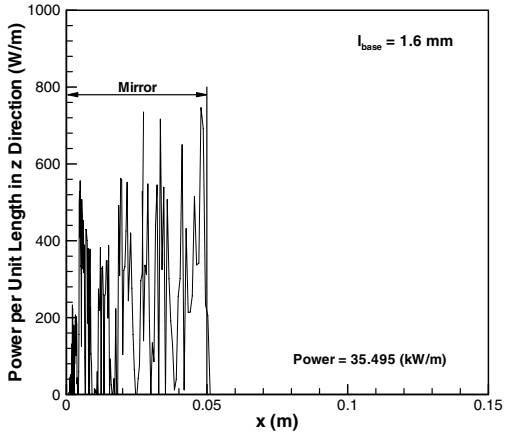

(c) Height of base = 1.6 *mm*

Fig. 15. Power distributions with respect to longitudinal distance x from the nozzle exit plane.

In order to get the high power laser beam, an appropriate condition for high gain should be achieved. As the base height decreases in the resonator, the maximum SSG becomes higher in the v_{1-0} transition, while it becomes lower for the v_{2-1}, v_{3-2} and v_{4-3} transitions except the vicinity of nozzle inlet. However, in this system, as the base height decreases, the extracted power is expected to be higher, because the v_{1-0} and v_{2-1} transitions more significantly contribute to the generation of high power laser beam compared with the other transitions [13].

Fig. 13 illustrates the maximum saturated gain distributions with respect to longitudinal distance x from the nozzle exit, when lasing occurs. The maximum saturated gain in the cavity is seen to vary within 0.65 regardless of its base height and vibrational transitions. Its reason is that the average gain in steady state must be a threshold value of

$$\alpha_{\text{average}} = -\frac{1}{2L_{\text{axis}}}\ln(r_0 r_{L_{\text{axis}}}). \tag{22}$$

Various DF distributions in transverse direction are seen in Fig. 14 at $x = 1$, 4 and 50 mm, which shows a width in which population inversion occurs in detail. While an axial position of $x = 1$ and 4 mm are located within the mirror, $x = 50$ mm corresponds to the other end of it. At $x = 1$ and 4 mm from the nozzle exit, the excited DF molecules in the upper energy level are observed to increase as the base height increases.

Variations of lasing power generated in the resonator are plotted in Fig. 15, which reveals that the peak power occurs in the vicinity of inlet as the base height decreases, since the chemical reaction is more intense therein. A higher power distribution in the latter part of mirror for base height of 1.6 mm is attributed to stronger population inversion in the v_{2-1} and v_{3-2} transitions as shown in Figs. 9 and 12. For the conditions listed in Table 1, the field temperature is not so high to generate the excited molecules in higher energy levels. The typical distribution of output power in the DF chemical laser was given by Spencer et al. [2] and it revealed that the v_{1-0} and v_{2-1} transitions are more important than the others. Also, in the present study, Figs. 9 and 14 show that it is more difficult to produce more DF(3) molecules than DF(1) or DF(2) molecules. That is, in the laser cavity, more DF(1) or DF(2) molecules exist in comparison with DF(3) molecules. Therefore, even if the maximum small signal gain in the v_{3-2} transition is higher than that in the v_{1-0} or v_{2-1} transition, the v_{1-0} or v_{2-1} transition is more important due to their high gain characteristics as well as wider and thicker high gain distributions. Consequently, the v_{1-0} and v_{2-1} transitions are considered to be more important in this system than the other transitions. As a result, the total laser beam power of each case is 37.585 kW/m for 0.4 mm base height, 35.828 kW/m for 0.8 mm and 35.495 kW/m for 1.6 mm. So, for the range of base height studied here, the total extracted power becomes higher as the base height decreases.

5. Concluding remarks

A numerical simulation of the DF chemical laser cavity has been performed by solving the full Navier–Stokes

equations, species equations and radiative transport equation. The effects of base height of the injector system on population inversion, gains, and lasing power have been investigated while discussing flow field characteristics in the DF chemical laser cavity. The base height was found to generate a recirculation zone that plays an important role in regulating the rates of mixing and chemical reaction behind the base in the DF chemical laser system. Further results have shown that

1. Both pressure and temperature become higher due to many shock wave interactions, as the base height decreases. Therefore, the chemical reaction and the population inversion are more activated in the cavity.
2. A reduction in F atom increases near the inlet region as the base height becomes smaller. However, the consumption of F atom decreases when lasing occurs due to the negative stimulated emission term in the energy equation.
3. The population inversion for the transition of DF(1)–DF(0) takes place in the whole cavity range while its strength becomes weaker as the base height increases. However, the transitions of DF(2)–DF(1) and DF(3)–DF(2) become stronger with an increase in base height. Correspondingly, as the base height decreases, the maximum SSG becomes higher for the v_{1-0} transition, whereas it becomes lower for the v_{2-1}, v_{3-2} and v_{4-3} transitions except for the vicinity of inlet.
4. The total extracted power becomes higher as the base height decreases, since the transition DF(1)–DF(0) plays a dominant role.

Acknowledgement

The financial assistance by the Combustion Engineering Research Center at KAIST is gratefully acknowledged.

References

[1] D.J. Spencer, H. Mirels, T.A. Jacobs, R.W.E. Gross, Preliminary performance of a CW chemical laser, Appl. Phys. Lett. 16 (6) (1970) 235–237.
[2] D.J. Spencer, H. Mirels, T.A. Jacobs, Comparison of HF and DF continuous chemical lasers: I. Power, Appl. Phys. Lett. 16 (10) (1970) 384–386.
[3] G. Emanuel, Analytical model for a continuous chemical laser, J. Quant. Spectrosc. Radiat. Transfer 11 (10) (1971) 1481–1520.
[4] W.S. King, H. Mirels, Numerical study of a diffusion-type chemical laser, AIAA J. 10 (12) (1972) 1647–1654.
[5] J.G. Skifstad, Theory of an HF chemical laser, Combust. Sci. Technol. 6 (1973) 287–306.
[6] J.E. Broadwell, Effect of mixing rate on HF chemical laser performance, Appl. Opt. 13 (4) (1974) 962–967.
[7] R. Tripodi, L.J. Coulter, B.R. Bronfin, L.S. Cohen, Coupled two-dimensional computer analysis of CW chemical mixing lasers, AIAA J. 13 (6) (1975) 776–784.
[8] J.D. Ramshaw, R.C. Mjolsness, O.A. Farmer, Numerical method for two-dimensional steady-state chemical laser calculations, J. Quant. Spectrosc. Radiat. Transfer 17 (1977) 149–164.
[9] R.J. Driscoll, Mixing enhancement in chemical lasers. Part I: Experiments, AIAA J. 24 (7) (1986) 1120–1126.
[10] R.J. Driscoll, Mixing enhancement in chemical lasers. Part II: Theory, AIAA J. 25 (7) (1987) 965–971.
[11] W. Hua, Z. Jiang, Y. Zhao, Nozzle design in CW hydrogen fluoride chemical laser, SPIE 2889 (1996) 135–140.
[12] M.L. Shur, The numerical analysis of HF chemical lasers in view of interference between the processes in the combustion zone and in nozzle unit, High Temp. Apparat. Struct. 37 (4) (1999) 647–655.
[13] R.W.F. Gross, J.F. Bott, Handbook of Chemical Lasers, John Wiley & Sons, New York, 1976.
[14] P.L. Roe, Approximate Riemann solvers, parameter vectors and difference schemes, J. Comput. Phys. 43 (1981) 357–372.
[15] H.C. Yee, Construction of explicit and implicit symmetric TVD schemes and their applications, J. Comput. Phys. 68 (1987) 151–179.
[16] H.C. Yee, A class of high resolution explicit and implicit shock-capturing methods, NASA TM 101099, 1989.
[17] A. Jameson, E. Turkel, Implicit schemes and LU decompositions, Math. Comput. 37 (156) (1981) 385–397.
[18] J.S. Park, Study of population inversion and laser beam generation in DF chemical laser system, Ph.D. thesis, Division of Aerospace Engineering, KAIST, 2005.